Journal of Power Sources 257 (2014) 319–324

Contents lists available at ScienceDirect

Journal of Power Sources

journal homepage: www.elsevier.com/locate/jpowsour

Surface modification of LiV_3O_8 nanosheets via layer-by-layer self-assembly for high-performance rechargeable lithium batteries

Runwei Mo [a], Ying Du [a,b], Naiqing Zhang [a,b], David Rooney [c], Kening Sun [a,b,*]

[a] Department of Chemistry, Harbin Institute of Technology, Harbin 150001, PR China
[b] Academy of Fundamental and Interdisciplinary Sciences, Harbin Institute of Technology, Harbin 150090, PR China
[c] School of Chemistry and Chemical Engineering, Queen's University Belfast, Belfast BT9 5AG, Northern Ireland, United Kingdom

HIGHLIGHTS

- The Al_2O_3-modified LiV_3O_8 nanosheets was prepared through self-assembly process.
- The thickness of the Al_2O_3 layer can be tuned by altering the layer-by-layer cycles.
- The cyclic stability and high rate capability are improved due to Al_2O_3 modifying.

ARTICLE INFO

Article history:
Received 18 December 2013
Received in revised form
15 January 2014
Accepted 28 January 2014
Available online 13 February 2014

Keywords:
Surface modification
Layer-by-Layer assembly
Lithium-ion battery
Cathode materials

ABSTRACT

In this work, an economical route based on hydrothermal and layer-by-layer (LBL) self-assembly processes has been developed to synthesize unique Al_2O_3-modified LiV_3O_8 nanosheets, comprising a core of LiV_3O_8 nanosheets and a thin Al_2O_3 nanolayer. The thickness of the Al_2O_3 nanolayer can be tuned by altering the LBL cycles. When evaluated for their lithium-storage properties, the 1 LBL Al_2O_3-modified LiV_3O_8 nanosheets exhibit a high discharge capacity of 191 mA h g^{-1} at 300 mA g^{-1} (1C) over 200 cycles and excellent rate capability, demonstrating that enhanced physical and/or chemical properties can be achieved through proper surface modification.

1. Introduction

Lithium-ion batteries (LIBs) are considered to be the most promising energy-storage systems for consumer electronics, hybrid electrical vehicles, and electrical vehicles (EV) because of their high power output, long cycle life, and high energy density [1–5]. Unfortunately, the power capability of LIBs is generally hindered by diffusion in micrometer-sized materials and/or bulk materials [6]. Nano-structured materials are becoming increasingly important in the field and hence have attracted great interest in recent years. This allows for shortening the Li^+-ion insertion distances and increase in electrode–electrolyte contact area [7] and thus enhancing the power density compared to micrometer-sized particles [8–11]. However, for nano-structured materials, increasing the electrode surface area of course allows for significantly more unfavorable side reactions (e.g., dissolution of species within the active material) [12,13].

Surface modification of electrode materials may not only promote faster Li^+ diffusion or electron transport but also suppress the side reactions [14–17]. Also, it has been demonstrated that engineering the morphology of LiV_3O_8 into one-dimensional (1D) and two-dimensional (2D) nanostructures (e.g., nanorods [18] and nanosheets [19]) facilitates the electron transport along the long dimension and Li^+ insertion/extraction along the lateral direction, and therefore enhanced electrochemical performances have been achieved. Inspired by this, we envision that the synergistic effects of nanostructuring and surface modification may contribute to the over kinetics of LiV_3O_8 as cathode materials for lithium-storage applications. Various processes, such as sol–gel [20] and heat treatment [21], have been developed to create artificial passivation layers on the surface of LiV_3O_8 particles. However, it remains a challenge to precisely control the coating thickness and uniformity with those processes. Thus it is the necessary to find a novel,

* Corresponding author. Academy of Fundamental and Interdisciplinary Sciences, Harbin Institute of Technology, Harbin 150001, PR China.
E-mail address: keningsunhit@126.com (K. Sun).

http://dx.doi.org/10.1016/j.jpowsour.2014.01.125
0378-7753/

scalable, cost-effective method to prepare the conformal coating thickness.

Layer-by-layer assembly (LBL) has recently attracted great attention as a promising method to form defect-free and highly conformal coatings [22,23]. The technique has advantages in chemically controlling the nanoscale local structure, film morphology, and thickness and incorporating a wide range of functional materials. Here we report on a facile LBL self-assembly approach combined with hydrothermal for the fabrication of Al_2O_3-modified LiV_3O_8 nanohybrids. The thickness of the Al_2O_3 nanolayer can be tuned by altering the LBL cycles. Such a LBL processing is environmentally friendly, versatile, and low cost, and therefore offers potential for scalability to create desirable surface-modified electrode materials. To the best of our knowledge, this is the first report on the Al_2O_3-modified LiV_3O_8 nanosheets through a LBL self-assembly process. More interestingly, the present Al_2O_3-modified LiV_3O_8 nanosheets, comprising a core of LiV_3O_8 nanosheets and a thin Al_2O_3 nanolayer, exhibit enhanced electrochemical lithium-storage performances.

2. Experimental

2.1. Synthesis of nanosized LiV_3O_8 powders

All chemicals used in our study were analytical grade and were used as received without further purification. In a typical synthesis, $LiOH{\cdot}H_2O$, NH_4VO_3, (V/Li = 3/1.00, mol) was mixed in distilled water under magnetic stirring and kept in a water bath at 80 °C for 1/2 h, and then a transparent solution was obtained. The resultant mixture was then transferred to a 50 mL autoclave and kept in an oven at 160 °C for 12 h. The resulting solution was heated overnight in an oven at 80 °C to produce the dry solid. The as-obtained material was calcined at 400 °C in air for 12 h.

2.2. Modification of nanosized LiV_3O_8 powders

Poly(diallyldimethylammonium chloride) (PDDA), Mw < 500 000 Da, and poly(sodium 4-styrenesulfonate) (PSS), Mw < 70 000 Da, were purchased from Alfa Aesar Co. Ltd. The as-synthesized nanosized LiV_3O_8 were first modified by polyelectrolyte (PDDA/PSS/PDDA) in sequence. Briefly, 30 mg of LiV_3O_8 nanoparticles was sonicated for 1 h in 50 mL of 1 M NaCl solution, and 80 mg of PDDA was added and stirred for 0.5 h. Subsequently, the excess PDDA was removed by six repeated centrifugation/wash cycles. Similarly, the following PSS and PDDA layers were then coated on the surface of the PDDA modified LiV_3O_8 nanoparticles sized to obtain the PDDA/PSS/PDDA modified LiV_3O_8 nanoparticles. The modified LiV_3O_8 nanoparticles were positively charged.

2.3. Synthesis ultrathin coatings on nanosized LiV_3O_8 powders

The PDDA/PSS/PDDA modified nanosized LiV_3O_8 powders were put into 50 mL of water with 0.1 g of $NaBH_4$, which were magnetic stirred for 2 min. Then, 0.02 g of $Al(NO_3)_3$ aqueous solution was slowly dropped into the above-mentioned solution at room temperature. After 0.5 h, the resulting white solid products were centrifuged, washed with distilled water and ethanol, and dried at 100 °C in air. Finally, the products were annealed at 400 °C in air for 5 h.

2.4. Characterizations

The resulting sample was characterized by means of X-ray diffraction (XRD, Rigaku D/max-γB) with monochromated Cu Kα radiation at a scanning rate of 2° min^{-1} in the range of 10–50°. Zeta-potential measurements were measured by electrophoretic light scattering spectrophotometer (ELS-8000). Morphology of products was characterized by scanning electron microscopy (SEM, Hitachi S4800) and high resolution transmission electron microscopy (HRTEM, JEM-2100) with an accelerating voltage of 200 kV.

2.5. Electrochemical measurements

The electrochemical measurements were carried out using two-electrode CR2025-type coin cells with pure lithium metal as both the counter and the reference electrodes at room temperature. The working electrode consisted of active material (e.g., 1 LBL-nLVO) was calculated at ca. 3.9 mg, a conductive agent (carbon black, Super-P), and a polymer binder (poly(vinylidene difluoride), PVDF, Aldrich) in a 80:10:10 weight ratio. The electrolyte used was 1.0 M $LiPF_6$ in ethylene carbonate (EC) and dimethyl carbonate (DMC) and diethyl carbonate (DEC) at a volumetric ratio of 1:1:1. Cell assembly was carried out in an Ar-filled glovebox with concentrations of moisture and oxygen below 1.0 ppm. The discharge–charge tests were conducted at various rates within a voltage window from 1.5 V to 4.0 V (vs. Li^+/Li) on the BTS battery testing system (Neware, Shenzhen, China).

3. Results and discussion

As schematically illustrated in Scheme 1, we first used layer-by-layer assembly to form a poly-electrolyte such as and poly(-diallyldimethylammonium chloride) (PDDA) and sodium poly(-styrenesulfonate) (PSS) on the surfaces of the nanosized LiV_3O_8 powders (nLVO). After adsorption of PDDA/PSS/PDDA, the surface charge of nLVO switched from negative (zeta pote ntial = −22 mV ± 1.5 mV) to positive (zeta potential = +41 mV ± 6.2 mV) (Fig. 1a). Secondly, the negatively charged BH_4^- was adsorbed onto the surface of the nLVO due to the electrostatic attraction between the charged species. Thirdly, a $Al(NO_3)_3$ solution was dropped into the above-mentioned solution; in this way, Al^{3+} was reduced into aluminum and then deposited onto the surface of the nLVO. Finally, the aluminum on the surface of the nLVO was oxidized into Al_2O_3 by calcinations in the air. Furthermore, thickness of Al_2O_3 coatings can be tuned by varying layer-by-layer assembly cycles.

X-ray diffraction (XRD) pattern of nLVO coated with Al_2O_3 via 1 LBL layer (1 LBL-nLVO) is displayed in Fig. 1b in comparison with that of bare nLVO (br-nLVO). All distinct XRD peaks from the sample of 1 LBL-nLVO are well indexed to the layered-type structure of

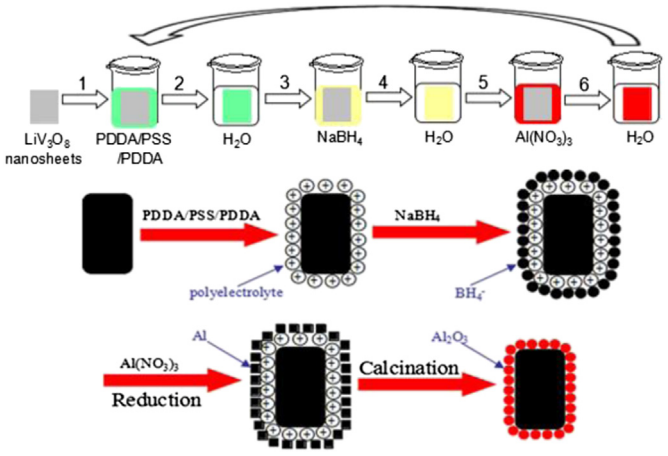

Scheme 1. Schematic representation for the preparation of the Al_2O_3-coated LiV_3O_8 nanoparticle by LBL.

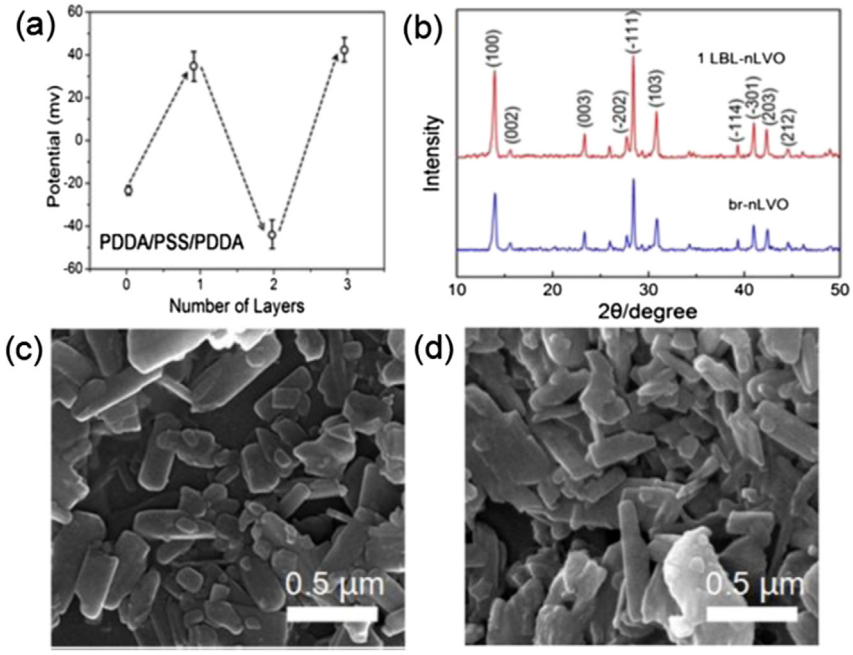

Fig. 1. (a) Zeta-potentials of LiV_3O_8 nanoparticles alternatively coated with PDDA/PSS/PDDA. (b) XRD patterns of bare LiV_3O_8 nanoparticles and LiV_3O_8 nanoparticles coated with 1 Al_2O_3 LBL layer. (c) and (d) SEM patterns of bare LiV_3O_8 nanoparticles and LiV_3O_8 nanoparticles coated with 1 Al_2O_3 LBL layer.

LiV_3O_8 with the P21/m space group (JCPDS 72-1193). The Al_2O_3 phase is not detectable even when nLVO coated with Al_2O_3 via 5 LBL layers (5 LBL-nLVO) (Fig. S1, ESI†), which can be ascribed to low weight ratio of Al_2O_3 [24]. Fig. 1c and d presents SEM images of br-LVO and 1 LBL-nLVO, respectively. As can be seen from Fig. 1c, nLVO has a particle-size distribution of approximately 100–300 nm. Fig. 1d shows the shape and morphology of 1 LBL-nLVO, which are almost identical to br-nLVO in Fig. 1c. There is no visible difference in the SEM image after the nLVO are coated with Al_2O_3 LBL film, possibly because the LBL coating is thin and highly-conformal and thus preserves the morphology of LiV_3O_8 nanosheet. Even when nLVO are coated with 5 Al_2O_3 LBL layers, the coated particles retain the same morphology and shape of bare particles as observed under SEM Fig. S2a (ESI†), suggesting the high conformality of LBL coating.

To study the details of LBL coatings, high-resolution TEM (HRTEM) is used to examine LBL-coated nLVO. Fig. 2b and c presents HRTEM images of br-nLVO and 1 LBL-nLVO. Comparison of the HR-TEM images of the br-nLVO (Fig. 2b) and 1 LBL-nLVO (Fig. 2c) also strongly supports conformal ultrathin layer of the coating. The lattice fringes in the surface region for br-nLVO (Fig. 2b) are identical to those in the bulk region. In contrast, conformal ~1.7 nm thick film which has clearly different lattice fringes from those in the bulk region is clearly observed for 1 LBL-nLVO (Fig. 2c). To obtain more information about LBL coatings, nLVO are coated with thicker Al_2O_3 LBL film (5 LBL) and are examined under TEM, as presented in Fig. S2b (ESI†). Fig. S2b (ESI†) clearly shows that a homogeneous LBL film is conformally coated on the crystalline nLVO. Thickness of the coating is estimated to ~8.5 nm. In order to confirm the deposition of Al_2O_3 on the surface of nLVO, energy dispersive X-ray spectroscopy (EDS) is used to examine the compositions at the center and the edge of 1 LBL-nLVO respectively, as shown in the inset graphs of Fig. 2a. Both EDS spectra reveal the elements of O, V, Al, and Cu. The Cu peaks are from the copper grid where the TEM sample is placed on. It is noted that the atomic percent of Al on the edge is 2.38%, larger than 1.27% in the center, confirming the formation of Al_2O_3 coating on the surface of nLVO. Therefore, we can conclude that Al_2O_3 LBL coatings are thin, dense, uniform, highly-conformal, and provide full coverage of nLVO.

Fig. 3a shows the initial charge/discharge curves of the br-nLVO, 1 LBL-nLVO and 5 LBL-nLVO electrodes at a current density of 300 mA g^{-1} (1C) in the voltage range of 1.5–4.0 V. It is apparent that the curves of all the electrodes are of resemblance, the apparent three discharge plateaus located at 2.85, 2.6 and 2.3 V, as we previously reported [25], can be well identified. The 2.8 V discharge plateau represents an electrochemical signature of single-phase insertion process [26], and the 2.6 V plateau is a signature of the two-phase transformation between $Li_{1+x}V_3O_8$ ($1 \leq x \leq 2$) and $Li_4V_3O_8$, while the last 2.3 V process, it concerns a slower kinetic insertion process [26–29]. Fig. 3a compares the charge–discharge cycling performance of br-nLVO, 1 LBL-nLVO and 5 LBL-nLVO electrodes when cycled between 1.5 and 4.0 V (vs Li/Li^+) at a current rate of 300 mA g^{-1} (1C). The capacity retention of br-nLVO is dramatically enhanced with 1 LBL and 5 LBL Al_2O_3 coatings resulting from nLVO on the electrode. And the br-nLVO loses almost all capacity after the same number of cycles. These results demonstrate that surface modification by Al_2O_3 LBL coatings can enhance cycling performances of nLVO cathodes. Furthermore, the effect of LBL coatings on the cycle ability of nLVO cathodes is dependent on the thickness of LBL coatings, which can be controlled precisely by varying LBL growth cycles. For example, nLVO cathode coated with Al_2O_3 LBL using 1 LBL cycle shows higher capacities and better cycle ability than the cathode coated with Al_2O_3 LBL using 5 LBL cycles, due to the reduced surface resistance of thinner Al_2O_3 coating. More interestingly, The 1 LBL-nLVO electrodes maintained a current density of ~300 mA g^{-1} with a Coulombic efficiency of 88.4% during the 200th cycle. After 200 cycles, the reversible capacity for 1 LBL-nLVO is still as high as 191 mA h g^{-1}, which is more than 2.3 times higher than that of the reversible capacity of br-nLVO (82 mA h g^{-1}). It seems that a thin coating of Al_2O_3 can improve the cyclic performance because the Al_2O_3 coating can prevent particles from agglomeration, meanwhile act as a shield to deter the irreversible phase transformation and protects the core material from direct contact with electrolyte [30].

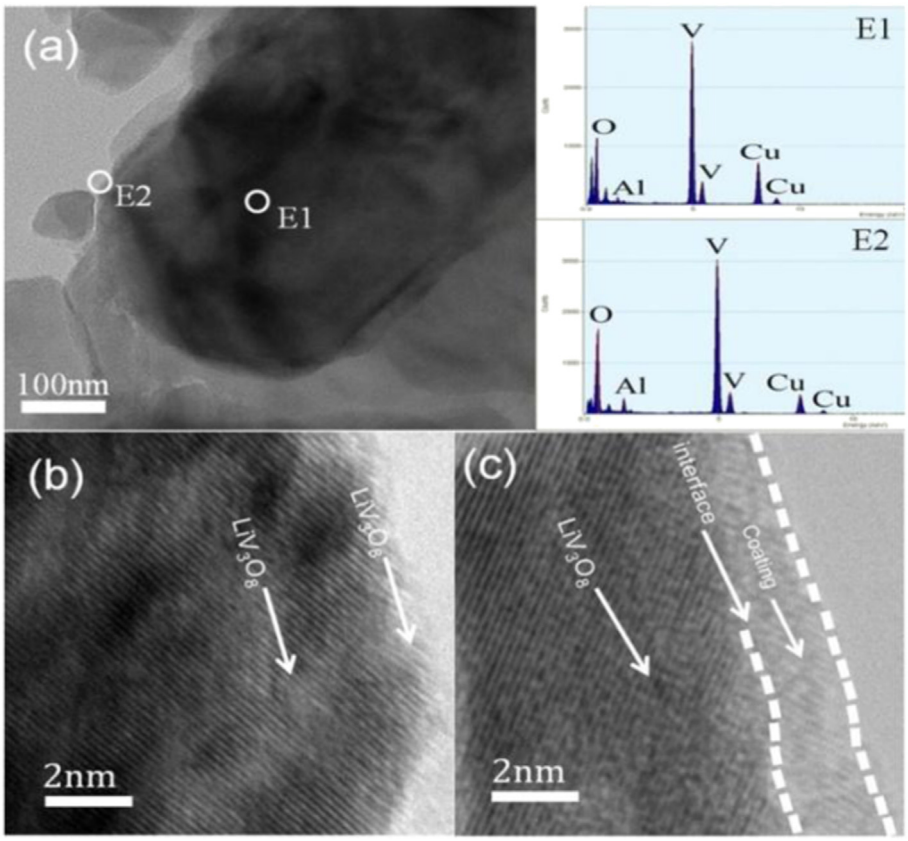

Fig. 2. (a) TEM image of LiV_3O_8 nanoparticles coated with 1 Al_2O_3 LBL layer. (b) The EDS signals of areas labeled as E1 and E2. (c) HRTEM images of bare LiV_3O_8 nanoparticles. (d) LiV_3O_8 nanoparticles coated with 1 Al_2O_3 LBL layer.

More exciting results come from the rate performance of the electrodes. Fig. 3b shows variations in discharge capacities versus charge–discharge cycle number for different nLVO electrodes cycled at different rates between 1.5 and 4.0 V (vs Li/Li^+) at room temperature. The improvement in the rate performance of the 1 LBL and 5 LBL Al_2O_3 coated LiV_3O_8 compared with that of the br-nLVO was due presumably to an inhibiting effect of the Al_2O_3 coating layer on the V dissolution from the LiV_3O_8 electrode to the

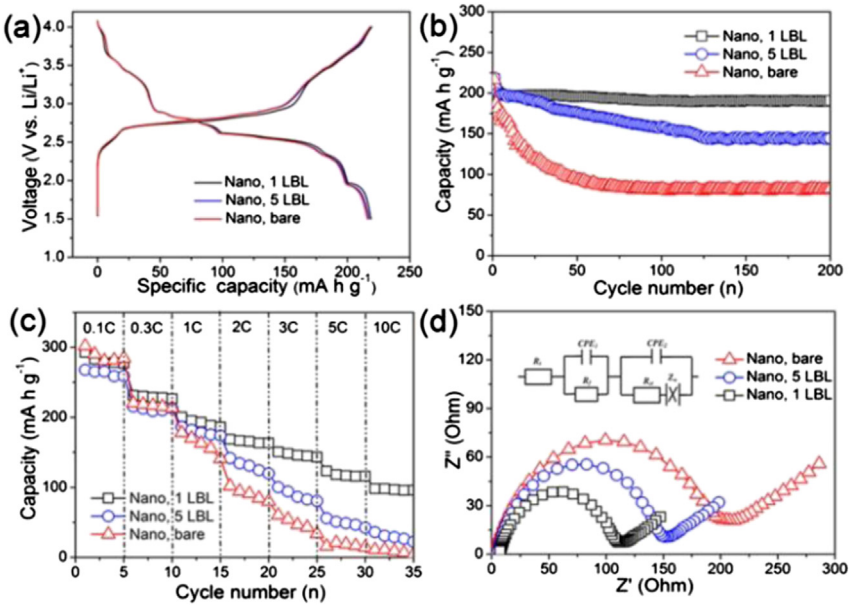

Fig. 3. (a) First-cycle discharge curves of the br-nLVO, 1 LBL-nLVO and 5 LBL-nLVO. (b) Cycling performance of the electrodes:br-nLVO, 1 LBL-nLVO and 5 LBL-nLVO. The electrodes were charged–discharged between 1.5 and 4 V (vs. Li/Li^+) at a rate of 300 mA g^{-1} (1C). (c) Rate-performance of the electrodes:br-nLVO, 1 LBL-nLVO and 5 LBL-nLVO. (d) Nyquist plots of the br-nLVO, 1 LBL-nLVO and 5 LBL-nLVO electrodes, the inset represents the equivalent circuit.

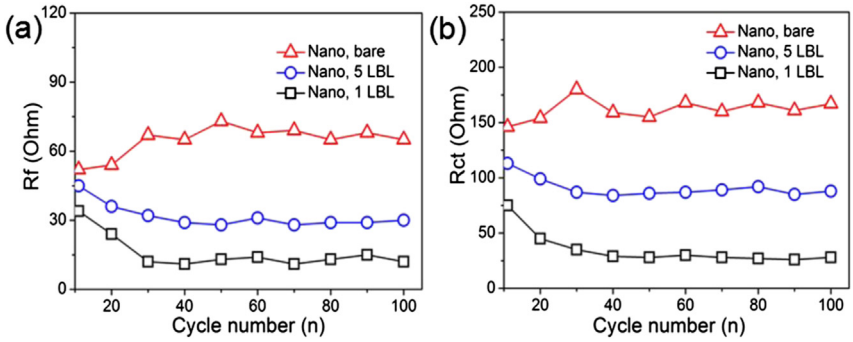

Fig. 4. Variation of (a) R_f and (b) R_{ct} during cycling calculated from fitting the Nyquist plots.

electrolyte. It is worth noting that the 1 LBL-nLVO have better rate-performance than the 5 LBL-nLVO. Considering that the difference in thickness of Al_2O_3 films between 1 LBL and 5 LBL cycles is between ~1.7 and ~8.5 nm, the decrease in rate-performance of 5 LBL-nLVO compared to 1 LBL-nLVO indicates that thick LBL Al_2O_3 coatings may result in poor Li^+ conductivity and further demonstrates the need for control of coatings thickness at the nanoscale.

To understand deeply the reasons for the excellent rate capability of the electrodes, electrochemical impedance spectroscopy (EIS) measurements were carried out for br-nLVO, 1 LBL-nLVO and 5 LBL-nLVO electrodes after the 10th cycle at a rate of 100 mA g^{-1}. Nyquist plots obtained from these three electrodes consist of one depressed semicircle at high/medium frequency and an inclined line at low frequency (Fig. 3d). In general, the semicircle is attributed to the summation of the contact, the solid-electrolyte interphase resistance, and the charge-transfer resistance, while the inclined line at ca. 45° angle to the real axis corresponds to the lithium-diffusion process within the electrodes. The impedance spectra are fitted with an equivalent circuit, where the symbols, R_s, R_f, R_{ct}, and Z_w, denote the solution resistance, contact resistance, charge-transfer resistance and Warburg impedance, respectively. The fitting results of R_s, R_f, and R_{ct} of sample br-nLVO, 1 LBL-nLVO and 5 LBL-nLVO (shown in Table S1, ESI†) indicate that the R_f and R_{ct} values of 1 LBL-nLVO composites are smaller than those of br-nLVO and 5 LBL-nLVO, indicating that the presence of thin coating significantly suppresses the rise of both of the surface film resistance and charge transfer resistance. Fig. 4 shows the different impedance values during the 10th and 100th cycles. It is clear that the R_f and R_{ct} of the 1 LBL-nLVO electrode have a similar trend, both decreasing from the 10th to the 30th cycle, then stabilizing around 12 Ω for R_f and 28 Ω for R_{ct}, indicating the formation of a stable surface layer and fast electron transportation. While in case of the br-nLVO electrode, the R_f and R_{ct} vary with ups and downs during cycling and mostly have higher values than those of 1 LBL-nLVO, indicating higher polarization of the electrode [31]. Furthermore, the fluctuations may be attributed to the absence of Al_2O_3 coating, which can restrict the thickening or deposition of SEI film during the charge/discharge processes [32,33]. Moreover, the well-dispersed particles, as shown in Fig. 1d, can favor in faster Li^+ diffusion and electron transportation, thus leading to a low value of R_{ct} for the 1 LBL-nLVO electrode. This is clear evidence that the 1 LBL-nLVO possess the highest electrical conductivity and the faster charge-transfer reaction for lithium ion insertion and extraction among all the samples, further confirming the synergistic effects of LiV_3O_8 nanostructuring and Al_2O_3 surface modification. The outstanding electrochemical performance of our 1 LBL-nLVO hybrid material for lithium ion batteries was attributed to the possible formation of the Li–V–Al–O solid solution at the LiV_3O_8/Al_2O_3 interface are of benefit to the electrochemical behaviors at high current densities. Enhanced Li^+ diffusion due to the formation of such a solid solution has also been reported for the formation of a $LiCo_{1-x}Al_xPO_z$ [34] or $LiCo_{1-x}Al_xO_z$ [35,36] solid solution. However, if the oxide coating is too thick, the capacities of the cathode material may be reduced because the oxide coating has higher electronic resistance and higher diffusion resistance for lithium ions. Hence, the 1 LBL Al_2O_3 coating not only can reduce the contact area of the charged active material with the electrolyte to protect the LiV_3O_8 particles from dissolving in the electrolyte, but also helps diminish charge-transfer resistance and the path length through which the electron and Li^+ion must travel within the electrode.

4. Conclusions

In summary, unique Al_2O_3-modified LiV_3O_8 nanosheets, comprising a core of LiV_3O_8 nanosheets and a thin Al_2O_3 nanolayer, were synthesized via a facile and economical route based on a hydrothermal process and layer-by-layer self-assembly. The thickness of the Al_2O_3 nanolayer can be tuned simply by controlling the concentrations of the precursor solutions or the LBL cycles. Compared to the LiV_3O_8 nanosheets, the Al_2O_3-modified LiV_3O_8 nanosheets show much better lithium-storage properties. The thickness of the Al_2O_3 nanolayer affects the electrochemical properties of the Al_2O_3-modified LiV_3O_8 nanosheets, demonstrating that enhanced physical and/or chemical properties can be obtained from proper surface modification. More importantly, the simple LBL process is broadly applicable and provides new strategies for the battery industry to design other novel nanostructured electrodes that are highly durable even while cycling at high rate.

Acknowledgements

This work was supported by the China Post-doctoral Science Foundation (2011M500650) and the Project (HIT.NSRIF. 2009087) supported by Natural Scientific Research Innovation Foundation in Harbin Institute of Technology.

Appendix A. Supplementary data

Supplementary data related to this article can be found at http://dx.doi.org/10.1016/j.jpowsour.2014.01.125.

References

[1] J. Maier, Nat. Mater. 4 (2005) 805.
[2] B. Dunn, H. Kamath, J.-M. Tarascon, Science 334 (2011) 928.
[3] M. Armand, J.-M. Tarascon, Nature 451 (2008) 652.
[4] B. Kang, G. Ceder, Nature 458 (2009) 190.
[5] X. Ji, K.T. Lee, L.F. Nazar, Nat. Mater. 8 (2009) 500.
[6] Y. Lee, M.G. Kim, J. Cho, Nano Lett. 8 (2008) 957.

[7] C.K. Chan, H. Peng, R.D. Twesten, K. Jarausch, X.F. Zhang, Y. Cui, Nano Lett. 7 (2007) 490.
[8] A.S. Arico, P. Bruce, B. Scrosati, J.M. Tarascon, T. Van Schalkwijk, Nat. Mater. 4 (2005) 366.
[9] P.L. Taberna, S. Mitra, P. Poizot, P. Simon, J.M. Tarascon, Nat. Mater. 5 (2006) 567.
[10] Y.G. Guo, Y.S. Hu, W. Sigle, J. Maier, Adv. Mater. 19 (2006) 2087.
[11] S.H. Lee, Y.H. Kim, R. Deshpande, P.A. Parilla, E. Whitney, D.T. Gillaspie, K.M. Kones, A.H. Mahan, S. Zhang, A.C. Dillon, Adv. Mater. 20 (2008) 3627.
[12] G.T.K. Fey, C.Z. Lu, J.D. Huang, T.P. Kumar, Y.C. Chang, J. Power Sources 146 (2005) 65.
[13] L. Xiao, Y. Yang, Y. Zhao, X. Ai, H. Yang, Y. Cao, J. Solid State Electrochem. 12 (2008) 149.
[14] K. Park, J. Son, H. Chung, S. Kim, C. Lee, K. Kang, H. Kim, Solid State Commun. 129 (2004) 311.
[15] C. Li, H.P. Zhang, L.J. Fu, H. Liu, Y.P. Wu, E. Rahmb, R. Holze, H.Q. Wu, Electrochim. Acta 51 (2006) 3872.
[16] W. Tang, X.W. Gao, Y.S. Zhu, Y.B. Yue, Y. Shi, Y.P. Wu, K. Zhu, J. Mater. Chem. 22 (2012) 20143.
[17] Q.T. Qu, Y.S. Zhu, X.W. Gao, Y.P. Wu, Adv. Energy Mater. 2 (2012) 950.
[18] A.Q. Pan, J. Liu, J.G. Zhang, G.Z. Cao, W. Xu, Z.M. Nie, X. Jie, D.W. Choi, B.W. Arey, C.M. Wang, S.Q. Liang, J. Mater. Chem. 21 (2011) 1153.
[19] A.Q. Pan, J.G. Zhang, G.Z. Cao, S.Q. Liang, C.M. Wang, Z.M. Nie, B.W. Arey, W. Xu, D.W. Liu, J. Xiao, G.S. Li, J. Liu, J. Mater. Chem. 21 (2011) 10077.
[20] L.L. Liu, X.J. Wang, Y.S. Zhu, C.L. Hu, Y.P. Wu, R. Holze, J. Power Sources 224 (2013) 290.
[21] L.F. Jiao, L. Liu, J.L. Sun, L. Yang, Y.H. Zhang, H.T. Yuan, Y.M. Wang, X.D. Zhou, J. Phys. Chem. C 112 (2008) 18249.
[22] G. Decher, Science 277 (1997) 1232.
[23] P.T. Hammond, Adv. Mater. 16 (2004) 1271.
[24] Y.K. Sun, K.J. Hong, J. Prakash, J. Electrochem. Soc. 150 (2003) A970.
[25] H.M. Liu, Y.G. Wang, K.X. Wang, Y.R. Wang, H.S. Zhou, J. Power Sources 192 (2009) 668.
[26] S. Jouanneau, A. Salle, A. Verbaere, D. Guyomard, J. Electrochem. Soc. 152 (2005) A166.
[27] J. Kawakita, T. Miura, T. Kishi, J. Power Sources 83 (1999) 79.
[28] J. Kawakita, T. Miura, T. Kishi, Solid State Ionics 120 (1999) 109.
[29] J. Kawakita, Y. Katayama, T. Miura, T. Kishi, Solid State Ionics 107 (1998) 145.
[30] W.-K. Kim, D.-W. Han, W.-H. Ryu, S.-J. Lim, H.-S. Kwon, Electrochim. Acta 71 (2012) 17.
[31] Y.Q. Qiao, X.L. Wang, Y.J. Mai, J.Y. Xiang, D. Zhang, C.D. Gu, J.P. Tu, J. Power Sources 196 (2011) 8706.
[32] Y.Q. Qiao, J.P. Tu, X.L. Wang, J. Zhang, Y.X. Yu, C.D. Gu, J. Phys. Chem. C 115 (2011) 25508.
[33] S.J. Shi, J.P. Tu, Y.Y. Tang, X.Y. Liu, Y.Q. Zhang, X.L. Wang, C.D. Gu, Electrochim. Acta 88 (2013) 671.
[34] A. Eftekhari, J. Electrochem. Soc. 151 (2004) A1456.
[35] J.D. Perkins, C.S. Bahn, J.M. McGraw, P.A. Parilla, D.S. Ginley, J. Electrochem. Soc. 148 (2001) A1302.
[36] Y.J. Kim, T.-J. Kim, J.W. Shin, B. Park, J. Cho, J. Electrochem. Soc. 149 (2002) A1337.